

Magnetotransport and internodal tunnelling in Weyl semimetals

G. Bednik,¹ K.S. Tikhonov,^{2,3} and S.V. Syzranov¹

¹*Physics Department, University of California, Santa Cruz, California 95064, USA*

²*L. D. Landau Institute for Theoretical Physics, 119334 Moscow, Russia*

³*Condensed-matter physics Laboratory, National Research University Higher School of Economics, 101000, Moscow, Russia*

Internodal dynamics of quasiparticles in Weyl semimetals manifest themselves in hydrodynamic, transport and thermodynamic phenomena and are essential for potential valleytronic applications of these systems. In an external magnetic field, coherent quasiparticle tunnelling between the nodes modifies the quasiparticle dispersion and, in particular, opens gaps in the dispersion of quasiparticles at the zeroth Landau level. We study magnetotransport in a Weyl semimetal taking into account mechanisms of quasiparticle scattering both affected by such gaps and independent of them. We compute the longitudinal resistivity of a disordered Weyl semimetal with two nodes in a strong magnetic field microscopically and demonstrate that in a broad range of magnetic fields it has a strong angular dependence $\rho(\eta) \propto C_1 + C_2 \cos^2 \eta$, where η is the angle between the field and the separation between the nodes in momentum space. The first term is determined by the coherent internodal tunnelling and is important only at angles η close to $\pi/2$. This contribution depends exponentially on the magnetic field, $\propto \exp(-B_0/B)$. The second term is weakly dependent on the magnetic field for realistic concentrations of the impurities in a broad interval of fields.

I. INTRODUCTION

Recent prediction¹ and experimental discovery²⁻⁴ of quasiparticles with Weyl dispersion in solid-state systems have motivated a vast number of predictions and observations of novel fundamental effects involving Weyl particles (see, e.g., Refs. 5 and 6 for a review). Some of these phenomena, such as the chiral anomaly⁷⁻⁹, rely on the transfer of quasiparticles between different Weyl nodes, sometimes also referred to as valleys, points in momentum space in whose vicinity the quasiparticles display Weyl dispersion.

Weyl nodes in solid-state systems come in pairs with opposite chiralities¹⁰. Apart from fundamental interest, internodal dynamics of Weyl quasiparticles may be used for valleytronic applications, i.e. using the valley degree of freedom to store, process and transfer information and to control electron transport¹¹. Experimentally observed manifestations of the internodal (intervalley) dynamics include also negative longitudinal magnetoresistance (see, e.g., Refs. 9, 12–20), a consequence of the chiral anomaly^{7,10}, and quantum oscillations of resistance in thin slabs of Weyl semimetals^{21,22} (WSMs). Changing the valley degree of freedom of quasiparticles has also been predicted to lead to the release or absorption of heat (“adiabatic dechiralisation”²³) and to affect the hydrodynamic flows of electrons in WSMs²⁴⁻³¹.

Of fundamental importance for valleytronic applications is coherent tunnelling between Weyl nodes. Such tunnelling leads to an effective coupling between the states of quasiparticles near different nodes, which may be controlled by the direction and the magnitude of an external magnetic field³². This coupling leads to the opening of a gap in the quasiparticle dispersion at the zeroth Landau level in WSMs^{32,33}, which has recently been observed in experiment³⁴⁻³⁶.

In this paper, we study the interplay of magnetotransport in disordered Weyl semimetals and coherent internodal

tunnelling. We demonstrate that the gap 2Δ , created in the quasiparticle dispersion by such tunnelling, affects significantly the longitudinal conduction (conduction along the magnetic field) of the quasiparticles if the magnetic field is perpendicular to the line connecting a pair of nodes in momentum space. Quasiparticle states are strongly hybridised between the nodes in this regime, and their scattering is affected by long-range correlated disorder, with the correlation length longer than the inverse separation between the nodes in momentum space. The longitudinal resistivity in this regime depends exponentially on the magnitude of the magnetic field.

For the other directions of the magnetic field, the internodal hybridisation of the quasiparticle states may be neglected. The resistivity is then determined by large-momentum scattering between states at different nodes and has a strong dependence on the direction of the field.

Our results demonstrate how the internodal coupling (the gaps in the spectra of Landau levels) in Weyl semimetals may be observed in transport experiments. Furthermore, strong dependence of the internodal coupling on the external magnetic field can be used in valleytronic devices to control electron transport if the magnetic field is perpendicular to the separation between the nodes.

The paper is organised as follows. In Sec. II we summarise our results for the magnetoconductance of a Weyl semimetal in a magnetic field. A detailed microscopic discussion of the model of a disordered two-node Weyl semimetal and its typical parameters is presented in Sec. III. We discuss the quasiparticle dispersion in the system in Sec. IV. Sections V and VI deal with quasiparticle scattering off impurities and magnetoconductance in disordered semimetals. In Sec. V we consider generic directions of the magnetic field where the magnetoresistance is weakly affected by the internodal coupling. Finally, in Sec. VI we demonstrate that the conduction is strongly affected by the coupling if the magnetic field is

perpendicular to the line connecting the nodes and compute the resistivity in this regime.

II. RESULTS

In the presence of an external magnetic field in a sufficiently clean system, the quasiparticle motion is quantised in the plane perpendicular to the field. At the zeroth Landau level, quasiparticles at each Weyl nodes may move only in one direction, either parallel or antiparallel to the magnetic field, depending on the chirality of the node, while quasiparticles at higher Landau levels may move both parallel and antiparallel to the magnetic field.

As a result, at strong magnetic fields or low levels of doping, for which only the zeroth Landau level contributes to transport (the *ultraquantum limit*), the longitudinal resistivity of a Weyl semimetal is determined by the internodal scattering. There are two main mechanisms of such internodal scattering: 1) large-momentum scattering between states at different nodes by impurities and 2) the interplay of small-momentum processes near one node and the internodal hybridisation of quasiparticle states.

In this paper, we analyse the dependence of the magnetoconductivity in a Weyl semimetal with two nodes as a function of the magnetic field B and its direction, focussing on the interplay of the internodal tunnelling and magnetoresistance. In the ultraquantum limit, the longitudinal resistivity of a Weyl semimetal with charged impurities may be described by the interpolation formula

$$\rho(\eta, B) = \rho_{\text{inter}} \cos^2 \eta + \rho_{\text{gap}}(B, \eta), \quad (2.1)$$

where $\rho_{\text{inter}} \cos^2 \eta$ is the contribution of large-momentum elastic scattering and is weakly dependent on the magnetic field; the last term $\rho_{\text{gap}}(B, \eta)$ accounts for the effects of the gap in the quasiparticle dispersion at the zeroth Landau level caused by coherent internodal tunnelling; η is the angle between the field and the separation between the nodes in momentum space.

For screened charged impurities, ubiquitous in Weyl and semiconducting systems, the function ρ_{inter} weakly depends on the magnetic field in the experimentally important limit $l_B Q \gg 1$, where l_B is the magnetic length and $2Q$ is the momentum separation between the nodes. By contrast, models with short-range scatterers are known to lead to linear magnetoresistance (see e.g. Refs. 37 and 38). Also, charged scatterers at very weak magnetic fields ($l_B Q \ll 1$) result in a different dependence of the resistivity ($\rho_{\text{inter}} \propto 1/B^2$) on the magnetic field³⁷. The strong angular dependence $\propto \cos^2 \eta$ of the first contribution in the resistivity (2.1) comes from the structure of the wavefunctions at the nodes.

The second contribution, $\rho_{\text{gap}}(B, \eta)$ is suppressed in the experimentally important case of weak magnetic fields and is, therefore, important at angles close to $\eta = \pi/2$. This contribution exhibits an exponential de-

pendence

$$\rho_{\text{gap}}(B, \pi/2) \propto \exp(-B_0/B) \quad (2.2)$$

on the magnitude of the magnetic field, where the characteristic field B_0 is given by the integral

$$B_0 = \frac{2c}{|e|v_F\hbar} \int_{\text{node 1}}^{\text{node 2}} \xi_{\mathbf{k}} dk \quad (2.3)$$

of the quasiparticle dispersion $\xi_{\mathbf{k}}$ along the minimum-action tunnelling path between the nodes in momentum space; v_F is the Fermi velocity which assumed to be isotropic near each node. The exponential dependence of the resistance (2.1) on the magnetic field comes from that of the gap³² in the dispersion of the quasiparticles, where the characteristic field B_0 may be on the order of $10T$ or larger³².

Away from the ultraquantum limit, i.e. at higher levels of doping or smaller magnetic fields, non-zero Landau levels contribute to the resistivity. Unlike the zeroth Landau level, quasiparticles at those higher Landau levels can be backscattered within the same node. Because of the long-range-correlated nature of the potential of screened impurities, such intranodal scattering at higher Landau levels is significantly stronger than the internodal scattering. The resistivity in this regime has recently been a subject of numerous studies (see, e.g., Refs. 7, 9, 39, and 40) and is not a focus of this paper.

At the levels of doping and magnetic fields where the higher Landau levels contribute to transport, their contribution $\rho_{\text{intra}}(B)$ to the resistivity may be added to the contributions (2.1) on which we focus in this paper. Different contributions may be separated from each other using their different dependencies on the direction and the value of the magnetic field. In the case of isotropic dispersions at Weyl nodes, the contribution $\rho_{\text{intra}}(B)$ of the intranodal scattering at high Landau levels is isotropic, which may be used to separate it from the first term in Eq. (2.1). It has also a weaker than exponential dependence on the magnetic field, which distinguishes it from the effects of the gap at the zeroth Landau level described by the second term in Eq. (2.1). For simplicity, in this paper we focus on the ultraquantum limit, where the contribution $\rho_{\text{intra}}(B)$ is absent and the full resistivity is, thus, described by Eq. (2.1).

We compute both contributions to the resistivity (2.1) microscopically. We find that for the experimentally important case of charged impurities and sufficiently small magnetic fields

$$\rho_{\text{inter}} = \frac{2\pi^3 n e^2}{v_F^2 Q^4 \hbar \varepsilon^2}, \quad (2.4)$$

where n is the concentration of the impurities and ε is the dielectric constant. For the gap-dependent contribution, which for the experimentally important case of low fields is relevant only at $\eta \approx \frac{\pi}{2}$ (or, equivalently, $\eta \approx -\frac{\pi}{2}$) we

obtain

$$\rho_{\text{gap}}\left(B, \frac{\pi}{2}\right) = C(B) \frac{nc|e|\hbar^2}{\mu_0^2 B_\mu^2} B \min\left[1, \left(\frac{B}{B_\mu}\right)^3\right] e^{-\frac{B_0}{B}}, \quad (2.5)$$

where $C(B)$ is a dimensionless coefficient weakly dependent on the magnetic field and where we introduced the characteristic magnetic field

$$B_\mu = \left(\frac{2\pi}{9\alpha}\right)^{\frac{1}{3}} \frac{c\mu_0^2}{|e|v_F^2\hbar}, \quad (2.6)$$

with $\alpha = \frac{e^2}{\varepsilon\hbar v_F}$ being the so-called fine-structure constant in a Weyl semimetal and μ_0 being the chemical potential in the system at zero magnetic field (measured from the energy of the Weyl node).

For a semimetal with the chemical potential $\mu_0 = 10\text{meV}$ (corresponding to the concentration of dopants $n \sim 10^{15}\text{cm}^{-3}$) and the dielectric constant^{41–44} $\varepsilon = 10 - 50$, the characteristic magnetic field B_μ lies, respectively, in the interval $B_\mu = 0.2 - 0.4\text{T}$. Fields of this order of magnitude correspond also to entering the ultraquantum limit for the characteristic chemical potentials under consideration. For such fields, the gap-dependent contribution $\rho_{\text{gap}}(B, \eta)$ is strongly suppressed, due to its exponential dependence on the magnetic fields, except for selected directions of the field, corresponding to $\eta = \pm\pi/2$. Thus, we expect our results for the contributions to Eq. 2.1 to hold in realistic Weyl semimetals for magnetic fields up to several tesla. For stronger fields, the resistivity is dominated by the gap-dependent contribution $\rho_{\text{gap}}(B, \eta)$ and has a strong exponential dependence on the magnetic field for all directions of the magnetic field (except $\eta = 0, \pi$, where the gap vanishes).

We emphasise that, although in most of this paper we consider a system with a single pair of Weyl nodes, our results may easily be generalised to the case of a system with multiple pairs of nodes, e.g., TaAs or TaP. The conductivity in such a system is given by the sum $\sigma(\mathbf{B}) = \sum_i [\rho_{\text{inter}} \cos^2 \eta_i + \rho_{\text{gap}}(B, \eta_i)]^{-1}$ of contributions from pairs of close nodes, where η_i is the angle between the field and the difference of momenta of the nodes in the i -th pair.

III. MODEL

We consider a Weyl semimetal (WSM) with two nodes separated along the z axis in momentum space. The Hamiltonian of the quasiparticles in this system, in the presence of charged impurities, is given by

$$\hat{H} = v_F \left(\hat{k}_x - \frac{e}{c} A_x\right) \hat{\sigma}_x + v_F \left(\hat{k}_y - \frac{e}{c} A_y\right) \hat{\sigma}_y + \hat{\sigma}_z m \left(\hat{k}_z - \frac{e}{c} A_z\right) + \frac{e^2}{\varepsilon} \sum_i Z_i \frac{e^{-\varkappa|\mathbf{r}-\mathbf{R}_i|}}{|\mathbf{r}-\mathbf{R}_i|}, \quad (3.1)$$

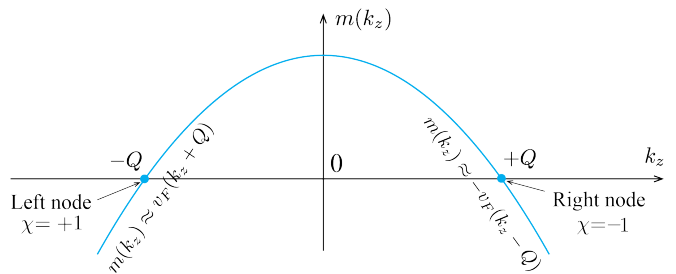


FIG. 1. (Colour online) The function $m(k_z)$ which determines the dispersion of the quasiparticles as a function of the momentum k_z for $k_x = k_y = 0$ [cf. Eq. (3.1)].

where the first three terms in the right-hand side (rhs) represent the kinetic energy of the quasiparticles in a magnetic field and the last term accounts for the potential of screened impurities; $\hat{\mathbf{k}} = (\hat{k}_x, \hat{k}_y, \hat{k}_z) = -i\partial_{\mathbf{r}}$ is the operator of the quasiparticle momentum (hereinafter $\hbar = 1$); $\hat{\sigma} = (\hat{\sigma}_x, \hat{\sigma}_y, \hat{\sigma}_z)$ is the pseudospin operator, a degree of freedom equivalent to a spin-1/2; the vector potential $\mathbf{A} = (A_x, A_y, A_z)$ accounts for the magnetic field; \mathbf{R}_i is the location of the i -th impurity; $Z_i e$ is the charge of the i -th impurity; \varkappa is the inverse screening length which is specified below; ε is the dielectric constant. For simplicity, we consider only two types of impurities, with $Z_i = +1$ (donors) and with $Z_i = -1$ (acceptors).

In Eq. (3.1) we introduced also a non-linear function $m(k_z)$ which may be approximated by the linear dependencies $m(k_z) \approx v_F (Q \mp k_z)$ near the Weyl nodes, located at the momenta $\mathbf{k} = (0, 0, \pm Q)$, as shown in Fig. 1, where the prefactor v_F is assumed, for simplicity, to match the velocity of the quasiparticles along the x and y axes in the absence of the magnetic field. The free quasiparticles, thus, have linear (Weyl) dispersions near the nodes with the velocity v_F and with opposite chiralities⁴⁵ $\chi = \pm 1$ at the respective nodes. The values of $m(k_z)$ away from the nodes determine the amplitude of quasiparticle tunnelling between the nodes in momentum space. Such tunneling is usually neglected in studies of transport in WSMs. In this paper, we demonstrate, however, that the internodal tunnelling has a qualitative effect on magnetotransport for certain directions of the magnetic field.

We choose the xz plane to be parallel to the direction of the magnetic field, as well as to the separation between the Weyl nodes in momentum space. In what follows, we use the Landau gauge

$$\mathbf{A} = (By \cos \eta, 0, -By \sin \eta), \quad (3.2)$$

where η is the angle between the direction of the magnetic field \mathbf{B} and the z axis, as shown in Fig. 3.

The magnetic field leads to the quantisation of the quasiparticle motion in the plane perpendicular to the field in a sufficiently clean system. While we expect our results to hold for arbitrary magnetic fields, we consider, for simplicity, the *ultra-quantum limit*, where only the

zeroth Landau level contributes to the transverse motion. This limit corresponds to sufficiently strong magnetic fields,

$$B > \frac{\mu^2 c}{2e^2 v_F^2}, \quad (3.3)$$

where μ is the chemical potential measured from the energy of the Weyl nodes. We assume also that Q is the largest momentum scale in the problem and, in particular, exceeds the inverse magnetic length

$$\frac{1}{l_B} = \sqrt{\frac{|e|B}{c}}. \quad (3.4)$$

Impurity potential. The last term in the Hamiltonian (3.1) describes the potential of the screened impurities. The inverse screening radius \varkappa is given, in the Thomas-Fermi approximation and in the ultra-quantum limit under consideration, by (see Appendix A for details)

$$\varkappa = \sqrt{\frac{2|e|^3 B}{\pi \epsilon v_F c}} \equiv \sqrt{\frac{2\alpha}{\pi}} \frac{1}{l_B}, \quad (3.5)$$

where l_B is the magnetic length, given by Eq. (3.4), and $\alpha = \frac{e^2}{v_F \epsilon}$ is the ‘‘fine-structure constant’’. Because the dielectric constant ϵ is large^{41–44} in most Weyl and Dirac materials, the fine-structure constant α may be assumed to be small, which justifies using the Thomas-Fermi approximation when describing electrostatic screening in these systems (see Appendix A for a more detailed discussion). A factor of 2 in Eq. (3.5) reflects the number of Weyl nodes in the system.

Donor and acceptor impurities affect the concentration of the quasiparticles and, thus, determine the chemical potential in the system. In an uncompensated system, i.e. at $n_A \neq n_D$, the chemical potential μ at realistic dopant concentrations may be considered homogeneous, with the average value significantly exceeding spatial fluctuations⁴⁶. Charge neutrality requires that

$$n_D - n_A = \frac{B|e|\mu}{2\pi^2 v_F c}, \quad (3.6)$$

where n_A and n_D are the concentrations of the acceptor and donor impurities. The right-hand-side part of Eq. (3.6) gives the concentration of quasiparticles measured from that in a disorder-free system with $\mu = 0$, which is related to the chemical potential μ_0 in the absence of the magnetic field as $n_D - n_A = \frac{\mu_0^3}{3\pi^2 v_F^3}$. Because the density of states of the charge carriers is affected by the magnetic field and their concentration $n_D - n_A$ is field-independent, the chemical potential μ depends on the magnetic field. According to Eq. (3.6),

$$\mu(B) = \frac{2c\mu_0^3}{3B|e|v_F^2}. \quad (3.7)$$

IV. QUASIPARTICLE DISPERSION IN A DISORDER-FREE SEMIMETAL

In this section, we analyse the dispersion of the quasiparticles at the zeroth Landau level in a disorder-free system. Figure 2 shows the dispersion, obtained by computing numerically the eigenenergies of the Hamiltonian (3.1) in the absence of impurities, as a function of the momentum $k_{z'}$ along the magnetic field and the angle η between the field and the separation between the nodes for η close to $\pi/2$.

The dispersion consists of two bands (the ‘‘upper band’’ and ‘‘lower band’’ in Fig. 2) separated by a gap 2Δ , which is determined by the internodal tunnelling of the quasiparticles. For $\eta = \pi/2$, the dispersion is particle-hole symmetric, i.e. the two branches of the dispersion are symmetric with respect to $E = 0$. For angles η deviating from $\pi/2$, the energies of both branches are shifted. At large momenta, $|k_{z'}| \gg \Delta/v_F$, the dispersion is linear as a function of momentum. In what follows, we describe the dispersion analytically.

A. Quasiparticle dispersion and wavefunctions for decoupled nodes ($\Delta = 0$)

First, we describe the dispersion and the wavefunctions of low-energy quasiparticles neglecting the internodal tunnelling. This corresponds to either a negligible gap 2Δ , e.g., due to the magnetic field being small, or to angles η sufficiently away from $\pi/2$, where the dispersion of low-energy quasiparticles (near the energy $E = 0$) is described by the linear parts of the dispersion branches, independent of the quantity Δ .

We linearise the function $m(k_z)$ in the Hamiltonian (3.1) near the node of chirality χ (cf. Fig. 1),

$$m(k_z) \approx v_F(Q + \chi k_z), \quad (4.1)$$

and rotate the coordinate frame by the angle η about the y axis, as shown in Fig. (3). The z' axis of the rotated coordinate frame $x'y'z'$ is parallel to the direction of the magnetic field \mathbf{B} and the components of the quasiparticle momenta in the $x'z'$ plane are given by

$$k_{x'} = k_x \cos \eta - k_z \sin \eta \quad (4.2)$$

$$k_{z'} = k_x \sin \eta + k_z \cos \eta. \quad (4.3)$$

It is convenient to rotate also the pseudospin basis at each node of chirality χ by the angle $\chi\eta$ about the y axis in the pseudospin space, which corresponds to the transformation of the Hamiltonian given by

$$\hat{H} \rightarrow \hat{H}' = e^{\frac{i\chi\eta\hat{\sigma}_y}{2}} \hat{H} e^{-\frac{i\chi\eta\hat{\sigma}_y}{2}}. \quad (4.4)$$

The Hamiltonian

$$\begin{aligned} \hat{H}'_0 = & v_F (Q \cos \eta + \chi k_{z'}) \hat{\sigma}_z \\ & + v_F \left(k_{x'} - \chi Q \sin \eta - \frac{e}{c} B y \right) - i v_F \partial_y \end{aligned} \quad (4.5)$$

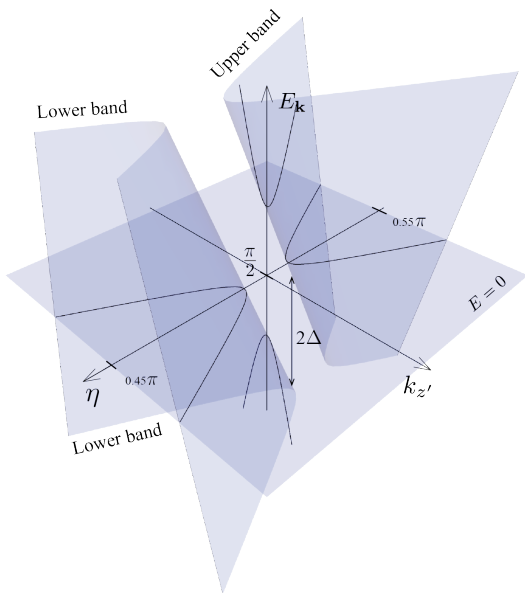


FIG. 2. (Colour online) The dispersion $E_{\mathbf{k}}$ of the quasiparticles in a Weyl semimetal in a magnetic field at the zeroth Landau level as a function of the momentum $k_{z'}$ along the magnetic field and the angle η between the field and the separation between the nodes for η close $\frac{\pi}{2}$. The dispersion has two bands, the “upper band” and the “lower band”. The “ $E = 0$ ” plane corresponds to the energies of the Weyl nodes in an undoped system.

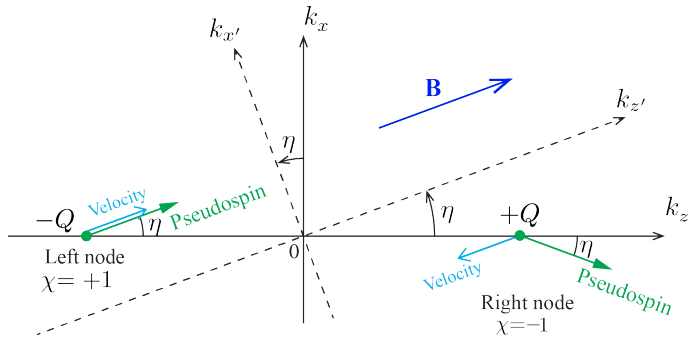


FIG. 3. (Colour online) Weyl nodes and the directions of the magnetic field, quasiparticle velocities and the pseudospins near the nodes.

of free quasiparticles near the nodes in the rotated pseudospin basis may be rewritten conveniently, by introducing the annihilation

$$\hat{a} = \frac{1}{l_B \sqrt{2}} \left(\partial_y + k_{x'} - \chi Q \sin \eta - \frac{e}{c} B y \right), \quad (4.6)$$

and creation \hat{a}^\dagger ladder operators of a harmonic oscillator,

in the form

$$\hat{H}'_0 = v_F (Q \cos \eta + \chi k_{z'}) \hat{\sigma}_z + \frac{1}{\sqrt{2}} \frac{v_F}{l_B} \hat{\sigma}^+ \hat{a}^\dagger + \frac{1}{\sqrt{2}} \frac{v_F}{l_B} \hat{\sigma}^- \hat{a}, \quad (4.7)$$

where $\hat{\sigma}^\pm = \hat{\sigma}_x \pm i \hat{\sigma}_y$.

The Hamiltonian (4.7) with the ladder operator (4.6) describes quasiparticles which propagate parallel (or antiparallel) to the z' axis, i.e. along the direction of the magnetic field \mathbf{B} , and whose motion in the transverse direction is quantised. The eigenstates of this Hamiltonian are parametrised by the component $k_{z'}$ of momentum parallel to the magnetic field, the number n of the Landau level of the transverse motion and the transverse component $k_{x'}$ of momentum. As discussed in Secs. II and III, we focus on the case of sufficiently strong magnetic fields, at which only the zeroth Landau levels contributes to transport.

The respective eigenstates of the Hamiltonian (4.7) are given by

$$|\psi_\chi\rangle = |\uparrow\rangle_\chi \otimes |0\rangle_{LL}(k_{x'}) \otimes |k_{z'}\rangle, \quad (4.8)$$

where $|\uparrow\rangle_\chi$ is the state of the pseudospin directed along the z axis in the pseudospin space [where the pseudospin basis depends on the chirality of the node χ , cf. (4.4)], $|0\rangle_{LL}$ is the eigenstate of the operator \hat{a} corresponding to the zeroth Landau level and parametrised by the momentum component $k_{x'}$ and $|k_{z'}\rangle$ describes a plane-wave wavefunction of a particle with momentum $k_{z'}$ along the z' axis. In the coordinate representation and the pseudospin basis of the Hamiltonian (3.1) the eigenstate is given by

$$\psi_{\chi\mathbf{k}}(\mathbf{r}) = e^{-\frac{(ck_{x'} - c\chi Q \sin \eta - eBy)^2}{2|e|B}} + ik_{z'} z' + ik_{x'} x' \left(\frac{|e|B}{\pi c L_{z'}^2 L_{x'}^2} \right)^{\frac{1}{4}} \begin{pmatrix} \cos \frac{\eta}{2} \\ \chi \sin \frac{\eta}{2} \end{pmatrix}, \quad (4.9)$$

where we assumed that the system has finite sizes $L_{z'}$ and $L_{x'}$ along the z' and x' axes; \mathbf{k} is the momentum in the xz plane (that matches the $x'z'$ plane). The energy of this eigenstate is determined by the first term in the effective Hamiltonian (4.7) and is given by

$$E_{\chi\mathbf{k}} = v_F (Q \cos \eta + \chi k_{z'}). \quad (4.10)$$

The pseudospins of the low-energy quasiparticles under consideration have different directions, shown in Fig. 3, at nodes of different chiralities χ . As follows from Eq. (4.10), the quasiparticle velocities $\mathbf{v}_{\chi\mathbf{k}} = \frac{\partial E_{\chi\mathbf{k}}}{\partial \mathbf{k}}$ at the nodes with $\chi = +1$ and $\chi = -1$ are, respectively, parallel and antiparallel to the magnetic field, as shown in Fig. 3.

1. Generic wavefunction near a node

Although the Hamiltonian lacks translational invariance in the presence of the magnetic field, a generic wavefunction, considered as a function of the momentum \mathbf{k} in

the xz plane and the coordinate y , may still be attributed to a particular node, so long as its generalised momentum $\mathbf{K} = \mathbf{k} - \frac{e}{c}\mathbf{A}$ is close to the momentum of this node in the absence of the magnetic field, where $\mathbf{A}(y)$ is the vector potential given by Eq. (3.2).

Indeed, this condition is equivalent to 1) the component $k_{z'}$ of the momentum being close to $-\chi Q \cos \eta$ and 2) the argument $k_z - \frac{e}{c}A_z$ of the function m in the Hamiltonian (3.1) being close to $-\chi Q$. The first condition guarantees that the wavefunction is a superposition of eigenstates with low energies (measured from the energy of a node), while the second condition allows us to linearise the function $m(k_z)$ according to Eq. (4.1).

B. Internodal tunnelling

The Hamiltonian (3.1) describes quasiparticles with a finite bandwidth along the z axis, which allows for quasiparticle tunnelling from one node to the other. Although this tunnelling is exponentially suppressed by this bandwidth, which exceeds all the other energy scales in the problem, it leads to the opening of the gap 2Δ , shown in Fig. 2, in the quasiparticle dispersion. In this subsection, we consider analytically the effect of such internodal tunnelling in momentum space on the quasiparticle dispersion and the opening of the gap.

The tunnelling leads to the hybridisation of low-energy quasiparticle states near different nodes. The generic wavefunction $\psi(\mathbf{r})$ of a quasiparticle with momentum components k_x and k_z in the xz plane and with a sufficiently low energy (measured from the energy of the nodes) may be approximated as a superposition of the wavefunctions (4.9) belonging to the nodes with $\chi = +1$ and $\chi = -1$.

Conditions for strong internodal hybridisation

Quasiparticle states at different nodes with the same momentum $k_{z'}$ are strongly hybridised by the internodal tunnelling if these states have the same energies in the absence of the tunnelling. Two quasiparticle states near the nodes with $\chi = +1$ and $\chi = -1$ have close energies (4.10) if the momentum $k_{z'}$ is sufficiently small. Because the energies under consideration are also small, this leads to the requirement of the smallness of the momentum scale $Q \cos \eta$ in comparison with the separation Q between the nodes in momentum space and the characteristic momentum scale associated with the internodal tunnelling discussed below.

Therefore, the states at different nodes may be strongly hybridised only for angles η sufficiently close to $\pi/2$,

$$\left| \eta - \frac{\pi}{2} \right| \ll \frac{\Delta}{v_F Q}, \quad (4.11)$$

where Δ is the characteristic coupling energy between the states with $\chi = +1$ and $\chi = -1$.

Strong hybridisation requires not only the angle η be close to $\pi/2$, but also the energies of the hybridised states be close to each other. At $\eta = \pi/2$, the energies of the states at nodes $\chi = +1$ and $\chi = -1$ are given by $E_{+1\mathbf{k}} = -E_{-1\mathbf{k}} = v_F k_{z'} = v_F k_x$, according to Eq. (4.10). Therefore, strong hybridisation of states between nodes requires also that

$$v_F |k_x| \ll \Delta, \quad (4.12)$$

in addition to the condition (4.11).

Internodal coupling

At angles η very close to $\pi/2$, i.e. for magnetic fields almost perpendicular to the separation between the nodes, the nodes are strongly coupled by the tunnelling and the effective Hamiltonian of low-energy quasiparticles is given by

$$\begin{aligned} \hat{\mathcal{H}}_{\text{internodal}}(\mathbf{k}) = & v_F (Q \cos \eta + k_{z'}) |\psi_{+1\mathbf{k}}\rangle \langle \psi_{+1\mathbf{k}}| \\ & + v_F (Q \cos \eta - k_{z'}) |\psi_{-1\mathbf{k}}\rangle \langle \psi_{-1\mathbf{k}}| \\ & + \Delta (|\psi_{+1\mathbf{k}}\rangle \langle \psi_{-1\mathbf{k}}| + |\psi_{-1\mathbf{k}}\rangle \langle \psi_{+1\mathbf{k}}|), \end{aligned} \quad (4.13)$$

where \mathbf{k} is the momentum in the xz plane, the states $|\psi_{\chi\mathbf{k}}\rangle$ are given by Eqs. (4.8) and (4.9), the first two lines describe the dispersion near decoupled nodes and Δ determines the strength of the coupling. At $\eta = \frac{\pi}{2}$ the quantity 2Δ gives the gap in the low-energy quasiparticle dispersion

$$E_{\mathbf{k}} = \pm (v_F^2 k_x^2 + \Delta^2)^{\frac{1}{2}} \quad (4.14)$$

shown in Fig. 2 (in the $\eta = \pi/2$ plane).

The amplitude of the tunnelling between the two nodes may be computed (see Appendix C) by matching the wavefunctions of the quasiparticles near the nodes with exponentially small ‘‘tails’’ between the nodes obtained in the quasiclassical approximation. Recently, the internodal coupling for a particular form of the function $m(k_z)$ [cf. Eq. (3.1)] has been computed in Ref. 32. In Appendix C, we generalise this calculation to the case of an arbitrary function $m(k_z)$, with the result

$$\Delta = v_F \sqrt{\frac{|e|B}{\pi c}} \exp \left[-\frac{c}{|e|B v_F} \int_{-Q}^Q m(k_z) dk_z \right]. \quad (4.15)$$

Equation (4.15) is valid for small values of the exponential, which reflects strong suppression of the quasiparticle wavefunctions away from the nodes. When deriving Eq. (4.15) we use also the smallness of the inverse magnetic length (3.4) compared to the separation $2Q$ between the nodes.

V. MAGNETOCONDUCTIVITY AWAY FROM

$$\eta = \pi/2$$

In this section, we consider magnetotransport for angles η away from $\pi/2$, at which the internodal tunnelling may be neglected and quasiparticles at different nodes are effectively decoupled. Because intranodal scattering processes do not change the velocities of the quasiparticles, shown in Fig. 3, the resistivity of the system in this regime is determined by the processes of internodal scattering.

As discussed in Sec. IV, the component \mathbf{k} of momentum in the xz plane is a good quantum number in a disorder-free system for the choice of the gauge of the vector potential given by Eq. (3.2). Internodal scattering occurs between quasiparticle states $\psi_{\chi\mathbf{p}}$ and $\psi_{-\chi\mathbf{k}}$ with momenta \mathbf{p} and \mathbf{k} separated by a vector of approximate length $2Q$. While the difference between the momenta of quasiparticles near different nodes is evident in the absence of magnetic field, it requires a clarification in the presence of a magnetic field due to the lack of translational invariance of the Hamiltonian.

Indeed, the change of the generalised momentum $\mathbf{k} - \frac{e}{c}\mathbf{A}(y)$ of a scattered quasiparticle is close to $2Q$. This leads to the difference between the incoming and outgoing momenta \mathbf{p} and \mathbf{k} being close to $2Q$ if the random potential is sufficiently smooth. The potential of the screened impurities is smooth at length scales shorter than the screening length $\kappa^{-1} \sim l_B/\alpha^{1/2}$. Therefore, the difference between the momenta \mathbf{p} and \mathbf{k} is close to $2Q$ so long as momentum scales on the order of $\alpha^{1/2}/l_B \ll Q$ are neglected. This conclusion may also be obtained by evaluating explicitly the matrix elements of scattering of the states of the form (4.9) on the potential of screened impurities (see Appendix D for details).

The scattering rate of the state $\psi_{\chi\mathbf{p}}$ at a node with chirality χ to the other node, with chirality $-\chi$, is given by

$$\frac{1}{\tau_{\chi\mathbf{p}}} = 2\pi \int \left\langle |\langle \psi_{\chi\mathbf{p}} | U | \psi_{-\chi\mathbf{k}} \rangle|^2 \right\rangle_{\text{dis}} \delta(E_{\chi\mathbf{p}} - E_{-\chi\mathbf{k}}) \frac{S_{xz} d\mathbf{k}}{(2\pi)^2}, \quad (5.1)$$

where U is the potential⁴⁷ of randomly located screened impurities; $\langle \dots \rangle_{\text{dis}}$ is our convention for the averaging over the locations of the impurities; $E_{\chi\mathbf{p}}$ is the energy of the state with momentum \mathbf{p} near node χ ; S_{xz} is the cross-sectional area of the system in the xz plane (which, for simplicity, is assumed to be constant along the y axis).

The potential $U(\mathbf{r})$ is given by the last term in the Hamiltonian (3.1) and is a sum of the potentials $u_i(\mathbf{r}) = Z_i \frac{e^2}{\epsilon} \frac{e^{-\kappa|\mathbf{r}-\mathbf{R}_i|}}{|\mathbf{r}-\mathbf{R}_i|}$ of individual impurities at locations \mathbf{R}_i . In this paper, we neglect single-particle interference effects related to scattering off multiple impurities^{48,49}, assuming that the concentration of impurities is small.

Under this approximation, we may make the replace-

ment

$$\begin{aligned} & \left\langle |\langle \psi_{\chi\mathbf{p}} | U(\mathbf{r}) | \psi_{-\chi\mathbf{k}} \rangle|^2 \right\rangle_{\text{dis}} \\ & \rightarrow \sum_i \frac{1}{V} \int d\mathbf{R}_i |\langle \psi_{\chi\mathbf{p}} | u(\mathbf{r} - \mathbf{R}_i) | \psi_{-\chi\mathbf{k}} \rangle|^2 \end{aligned} \quad (5.2)$$

in the expression (5.1) for the scattering time. Using Eq. (5.2) and evaluating the integral in Eq. (5.1) (see Appendix D for the details), we arrive at the internodal scattering rate

$$\frac{1}{\tau} \approx \frac{2\pi n |e|B}{v_{FC}} \left(\frac{e^2 \cos \eta}{2\epsilon Q^2} \right)^2, \quad (5.3)$$

which is independent of the momentum of the scattered quasiparticle, where $n = N/V$ is the concentration of the impurities in the system.

The dependence $\propto \cos^2 \eta$ of the scattering rate on the angle η reflects the projection of the pseudospins of quasiparticles at different nodes, shown in Fig. 3, onto each other. Equation (5.3) suggest that the internodal scattering vanishes at $\eta = \pi/2$ as the pseudospins at different nodes are opposite to each other if the magnetic field is perpendicular to the line separating the nodes. We emphasise, however, that the result (5.3) for the scattering rate applies at angles η which are not very close to $\pi/2$, at which the hybridisation between quasiparticle states at different nodes becomes may be neglected.

Because the quasiparticles in an impurity-free system move parallel to the magnetic field, the longitudinal conductivity (along the magnetic field) of a weakly disordered system exceeds significantly its transverse conductivity. When computing the longitudinal conductivity, on which we focus in this paper, transport may, therefore, be considered to be one-dimensional, with $N_{\perp} = \frac{|e|B}{2\pi c}$ transverse channels per cross-sectional unit area.

Since conduction comes only from low-energy quasiparticles, with energies significantly exceeded by the bandwidth, their distribution function $f(k_{x'}, k_{z'}, \mathbf{r})$ in the space of the momentum $\mathbf{k} = (k_{x'}, k_{z'})$ in the xz plane and 3D coordinates \mathbf{r} is peaked sharply near the surfaces $k_{z'} = -\chi Q \cos \eta$; $k_{x'} = \chi Q \sin \eta + \frac{eB}{c}y$, corresponding to node χ , according to the discussion in Sec. IV A 1. Because the dynamics of the quasiparticles is effectively one-dimensional and confined to the zeroth Landau level in the transverse direction, it is convenient to introduce the distribution function $F(k_{z'}, \mathbf{r}) = \int_{\chi} \frac{dk_{x'}}{2\pi} f(k_{z'}, k_{x'}, \mathbf{r})$ of the longitudinal momentum $k_{z'}$ and coordinate near node χ , where the integration with respect to the momentum $k_{x'}$ is carried out near that node.

The dynamics of this distribution function is governed by the kinetic equation

$$\begin{aligned} \frac{\partial F_{\chi}(k_{z'}, \mathbf{r})}{\partial t} + \chi v_F \frac{\partial F_{\chi}(k_{z'}, \mathbf{r})}{\partial z'} + e E_{z'} \frac{\partial F_{\chi}(k_{z'}, \mathbf{r})}{\partial k_{z'}} \\ = \frac{F_{-\chi}(-k_{z'}, \mathbf{r}) - F_{\chi}(k_{z'}, \mathbf{r})}{\tau} \end{aligned} \quad (5.4)$$

for momenta $k_{z'}$ close to the value $k_{z'} \approx \pm Q \cos \eta$ near a node of chirality χ . Equation (5.4) reflects that elastic internodal scattering leads to the scattering of states with momentum $k_{z'}$ along the z' axis into the states with momentum $-k_{z'}$, as follows from the conservation of energy (4.10).

The generic stationary solution of the kinetic equation (5.4) in a homogeneous system in the presence of a small electric field $E_{z'}$ is given by

$$F_{\chi}(k_{z'} + eE_{z'}\tau) = F_{-\chi}(-k_{z'}), \quad (5.5)$$

which leads to the current in the z' direction

$$j = eN_{\perp}v_F \int [F_{+1}(k_{z'}) - F_{-1}(k_{z'})] \frac{dk_{z'}}{2\pi} = \frac{|e|^3 v_F B \tau}{(2\pi)^2 c} E_{z'}, \quad (5.6)$$

Utilising Eqs. (5.6) and (5.3) and recovering the Planck's constant \hbar we arrive at the conductivity

$$\sigma_{\text{inter}} = \frac{v_F^2 Q^4 \hbar \varepsilon^2}{2\pi^3 n e^2} \frac{1}{\cos^2 \eta}, \quad (5.7)$$

which describes the first contribution to the resistivity in Eq. (2.1) with ρ_{inter} given by (2.4).

As discussed in Sec. II, the conductivity (5.7) is weakly dependent on the magnetic field and exhibits strong anisotropy, i.e. strong dependence on the magnetic field. A strong dependence of the conductivity on the direction of the magnetic field has also been noted in Ref. 50, however, with a different dependence on the direction. We believe that the difference comes from assuming in Ref. 50, without a derivation for a particular model, a certain structure of the kinetic energy and the disorder potential in the space of the nodal spin. We emphasise also that the absence of the dependence of the conductivity (5.7) on the amplitude of the magnetic field is specific to charged impurities considered here and sufficiently strong fields corresponding to $Ql_B \gg 1$. By contrast, models with short-ranged impurities have been demonstrated (see, e.g., Refs. 37, 38, and 50) to exhibit linear magnetoresistivity.

VI. MAGNETOCONDUCTIVITY AT ANGLES η CLOSE TO $\pi/2$

In this section, we consider magnetotransport at angles η close to $\pi/2$, i.e. for the magnetic field \mathbf{B} parallel to the x axis. In this case, quasiparticle states at different nodes are coupled strongly by the internodal tunnelling. As discussed in Sec. V, the internodal coupling determines essentially the resistivity in this regime, as the conductivity (5.7) diverges at $\eta = \pi/2$.

We assume here that the chemical potential μ (measured from the energy of the Weyl nodes in the absence of the magnetic field) is greater than the internodal coupling Δ . Indeed, the chemical potential μ is on the order

of several dozen meV for typical doping levels in WSMs (see, e.g., Refs. 51–53), whereas the coupling is of order several meV for fields $B \sim 10T$ and decreases exponentially for smaller fields.

In this approximation, the quasiparticle states in the absence of disorder may be represented in the form

$$|\phi_{\chi\mathbf{k}}\rangle \approx |\psi_{\chi\mathbf{k}}\rangle + \frac{\chi\Delta}{2v_F k_x} |\psi_{-\chi\mathbf{k}}\rangle, \quad (6.1)$$

as follows from the effective Hamiltonian (4.13) of the quasiparticles at $\eta = \pi/2$. The second term in Eq. (6.1) is small, due to the smallness of the parameter $\Delta/(k_x v_F) \ll 1$, and accounts for the hybridisation between the states $|\psi_{+1\mathbf{k}}\rangle$ and $|\psi_{-1\mathbf{k}}\rangle$ due to internodal tunnelling, which is essential for the conductivity being finite at $\eta = \pi/2$.

Quasiparticles with the wavefunctions $|\phi_{+1\mathbf{k}}\rangle$ and $|\phi_{-1\mathbf{k}}\rangle$ move with the velocity v_F (up to small corrections on the order of Δ^2/μ^2), respectively, parallel and antiparallel to the x axis. The resistivity of the system is, thus, determined by the processes of scattering between the states $|\phi_{\chi\mathbf{k}}\rangle$ with different χ .

The respective ‘‘internodal’’ scattering rate is given by Eq. (5.1) with the replacement $|\psi_{\chi\mathbf{k}}\rangle \rightarrow |\phi_{\chi\mathbf{k}}\rangle$. Utilising Eqs. (5.1), (5.2), (6.1) and (4.10), we obtain the scattering rate (see Appendix E for details)

$$\frac{1}{\tau} \approx \frac{2\pi n v_F e^4}{\varepsilon^2 [4\mu^2(B) + \varkappa^2(B)v_F^2]} \frac{\Delta^2}{\mu^2(B)} \left[1 + I \left(l_B Q, l_B \sqrt{4\mu^2(B) + \varkappa^2 v_F^2 / v_F} \right) \right], \quad (6.2)$$

where the function $I(s, t)$ is given by

$$I(s, t) = \frac{t^2}{\pi} \int \frac{\cos(2sy) e^{-\frac{z^2+y^2}{2}}}{(y^2 + z^2 + t^2)^2} dz dy \quad (6.3)$$

and the chemical potential $\mu(B)$ is given by Eq. (3.7). Depending on the values of the magnetic field and the chemical potential, the value of the function $I(l_B Q, l_B \sqrt{4\mu^2(B) + \varkappa^2 v_F^2 / v_F})$ may vary from zero, in the limit $Ql_B \max\left(\sqrt{\frac{2\alpha}{\pi}}, \frac{2\mu l_B}{v_F}\right) \gg 1$, to unity, in the limit $Ql_B \max\left(\sqrt{\frac{2\alpha}{\pi}}, \frac{2\mu l_B}{v_F}\right) \ll 1$ (see Appendix E for details).

For the experimentally relevant case of chemical potentials $|\mu(B)| \gg \Delta$ exceeding the gap Δ in quasiparticle dispersion, the quasiparticles move with velocities v_F and $-v_F$ along the z' axis and the conductivity of the system is given by the same expression

$$\sigma = \frac{|e|^3 v_F B}{(2\pi)^2 c} \tau \quad (6.4)$$

as in Sec. V [cf. Eq. (5.6)]. Equations (6.2) and (6.4) give the longitudinal conductivity of a WSM in a magnetic

field perpendicular to the line connecting the nodes in the form

$$\sigma = \frac{\varepsilon^2 B (\mu^2 + \varkappa^2 v_F^2) \mu^2}{(2\pi)^3 n |e| c (1 + I) \Delta^2}, \quad (6.5)$$

where $I = I(l_B Q, l_B \sqrt{4\mu^2(B) + \varkappa^2 v_F^2} / v_F)$ and Δ is the gap in the dispersion of the quasiparticles at the zeroth Landau level given by Eq. (4.15).

In what immediately follows, we provide the results for conductivity in the two limiting cases: $\mu \gg \varkappa v_F$ and $\mu \ll \varkappa v_F$. According to Eqs. (3.5) and (3.7), this corresponds, respectively, to the magnetic fields $B \ll B_\mu$ and $B \gg B_\mu$, where the characteristic field B_μ is given by Eq. (2.6) and is on the order of $0.1T$ for typical Weyl semimetals. For $B \ll B_\mu$, Eq. (6.4) gives

$$\sigma = \frac{2\varepsilon^2 c^4 \mu_0^{12}}{81\pi^2 n e^6 v_F^{10} (1 + I)} \frac{1}{B^4} \exp \left[\frac{2c}{|e| B v_F} \int_{-Q}^Q m(k_z) dk_z \right]; \quad (6.6)$$

for $B \gg B_\mu$

$$\sigma = \frac{\varepsilon c \mu_0^6}{9\pi^3 n |e| v_F^5 (1 + I)} \frac{1}{B} \exp \left[\frac{2c}{|e| B v_F} \int_{-Q}^Q m(k_z) dk_z \right]. \quad (6.7)$$

Combining Eqs. (6.6) and (6.7) and recovering the Planck's constant \hbar gives the interpolation formula (2.5).

VII. ACKNOWLEDGMENTS

We are grateful to Ya.I. Rodionov for useful discussions and previous collaboration on related topics. Our work has been supported financially by the Hellman Foundation and the Faculty Research Grant awarded by the Committee on Research from the University of California Santa Cruz (SVS) and by the Basic Research Programme of the HSE University (KST).

Appendix A: Screening of impurities in a strong magnetic field

In this section, we discuss the screening of a charged impurity in a Weyl semimetal in the presence of a magnetic field. The electrostatic potential ϕ around an impurity of charge Ze located at $\mathbf{r} = 0$ is given by

$$\varepsilon \Delta\phi(\mathbf{r}) = 4\pi Ze \delta(\mathbf{r}) + 4\pi en(\mathbf{r}), \quad (\text{A1})$$

where $n(\mathbf{r})$ is the change of the density of the electrons due to exposing the system to the potential ϕ at location \mathbf{r} . In the Thomas-Fermi approximation⁴⁸, the response of the electron density $n(\mathbf{r})$ to the potential $\phi(\mathbf{r})$ is local, which gives

$$n(\mathbf{r}) = N_{\text{nodes}} \frac{|e|B}{2\pi c} \int \frac{dk_z}{2\pi} \{n_F[v_F k_z - e\phi(\mathbf{r})] - n_F(v_F k_z)\} = -N_{\text{nodes}} \frac{e^2 B \phi}{(2\pi^2) c v_F}, \quad (\text{A2})$$

where $\frac{|e|B}{2\pi c}$ accounts for the degeneracy of the Landau level; $v_F k_z$ is the dispersion of the quasiparticle along the magnetic field; N_{nodes} is the number of Weyl nodes in the system (in the rest of the paper, $N_{\text{nodes}} = 2$) and $n_F(\varepsilon)$ is the Fermi-Dirac distribution function.

Equations (A1) and (A2) describe linear screening with the radius \varkappa^{-1} which for $N_{\text{nodes}} = 2$ is given by Eq. (3.5). We note that the impurity screening may be neglected when considering the direct internodal scattering, because the change of momentum for such scattering processes is close to $2Q$ and exceeds significantly the screening constant \varkappa . Therefore, our results for the conductivity obtained in Sec. V, e.g., Eqs. (2.4) and (5.7), are independent of the model of screening.

The screening and the details of the screened potential may be important, however, when considering the transport of quasiparticle states strongly hybridised between the nodes. The respective contribution to the resistivity, considered in Sec. VI, is determined by small momentum scattering on the order of $\min(|\mu|/v_F, \varkappa)$, where μ is the chemical potential in the system.

Thomas-Fermi approximation, which we used to obtain Eq. (A2) and the form of the screened potential given by the last term of the Hamiltonian (3.1), is justified provided the screening length \varkappa^{-1} exceeds the characteristic lengths of the wavefunctions of the electrons which provide screening: the magnetic length l_B and the wavelength v_F/μ corresponding to the motion along the field. The condition $\varkappa^{-1} \gg l_B$ is fulfilled in typical Weyl semimetals due to the smallness of the ‘‘fine structure constant’’ discussed in Sec. III. According to Eqs. (3.5) and (3.7), the condition

$$\varkappa^{-1} \gg v_F/\mu \quad (\text{A3})$$

is fulfilled so long as the magnetic field B is significantly smaller than the characteristic value given by Eq. (2.6). The Thomas-Fermi approximation, used here, breaks down if the magnetic field exceeds this characteristic value, which may affect the pre-exponential in Eq. (6.7) and in Eq. (2.5) in the limit $B \gg B_\mu$, however, the results should still be expected to hold qualitatively.

Appendix B: Landau levels of electrons near decoupled nodes

In this section, we present a detailed derivation of the wavefunctions of quasiparticle near each Weyl node neglecting the internodal tunnelling. The Hamiltonian of a disorder-free Weyl semimetal with two nodes and the quasiparticle dispersion linearised near the nodes is given by

$$\hat{H}_0 = v_F \left(k_x - \frac{e}{c} B y \cos \eta \right) \hat{\sigma}_x - i v_F \hat{\sigma}_y \partial_y + v_F \left(Q + \chi k_z + \chi \frac{e}{c} B y \sin \eta \right) \hat{\sigma}_z, \quad (\text{B1})$$

where the momenta k_x and k_z along the x and z axes are good quantum numbers. The eigenfunction $\psi_{k_x k_z \chi}$ of a quasiparticle at node χ and its eigenstate $E_\chi^2(k_x k_z)$ satisfies the equation $\hat{H}_0^2 \psi_{k_x k_z \chi} = E_\chi^2(k_x k_z) \psi_{k_x k_z \chi}$, where the operator \hat{H}_0^2 is given by

$$\hat{H}_0^2 = v_F^2 \left[-\partial_y^2 + \left(k_x - \frac{e}{c} B y \cos \eta \right)^2 + \left(Q + \chi k_z + \frac{e}{c} \chi B y \sin \eta \right)^2 \right] + \frac{e}{c} B v_F^2 (\hat{\sigma}_z \cos \eta + \chi \hat{\sigma}_x \sin \eta). \quad (\text{B2})$$

After performing the transformation of the pseudospin basis given by Eq. (4.4) and the rotation of the coordinate frame given by Eqs. (4.2) and (4.3), the operator $(\hat{H}'_0)^2$, given by Eq. (B2), takes the form

$$\left(\hat{H}'_0 \right)^2 = v_F^2 \left\{ -\partial_y^2 + \left(k_{x'} - \chi Q \sin \eta - \frac{e}{c} B y \right)^2 + (k_{z'} + \chi Q \cos \eta)^2 + \frac{e}{c} B \hat{\sigma}_z \right\}. \quad (\text{B3})$$

The operators (B2) and (B3) have the form of the Hamiltonian of a system consisting of a one-dimensional harmonic oscillator with the mass $1/2v_F^2$ and the frequency $2v_F^2|e|B/c$ and an independent spin-1/2 in a magnetic field. To obtain the eigenstates of the system, it is convenient, therefore, to introduce the ladder operators

$$\hat{a}^\dagger = \sqrt{\frac{c}{2|e|B}} \left(-\partial_y + k_{x'} - \chi Q \sin \eta - \frac{e}{c} B y \right), \quad (\text{B4})$$

$$\hat{a} = \sqrt{\frac{c}{2|e|B}} \left(\partial_y + k_{x'} - \chi Q \sin \eta - \frac{e}{c} B y \right) \quad (\text{B5})$$

of this harmonic oscillator.

In terms of the creation and annihilation operators \hat{a}^\dagger and \hat{a} , given by Eqs. (B4) and (B5), the Hamiltonian of the quasiparticles in the rotated pseudospin basis has the form

$$\hat{H}'_0 = v_F (Q \cos \eta + \chi k_{z'}) \hat{\sigma}_z + \frac{1}{\sqrt{2}} \frac{v_F}{l_B} \hat{\sigma}^+ \hat{a}^\dagger + \frac{1}{\sqrt{2}} \frac{v_F}{l_B} \hat{\sigma}^- \hat{a}. \quad (\text{B6})$$

The eigenstates and the eigenenergies of the Hamiltonian (B6), corresponding to the zeroth Landau level, are given, respectively, by Eqs. (4.8) and (4.10).

Appendix C: Intervalley coupling for $\eta = \pi/2$

In this section, we present an explicit calculation of the internodal coupling Δ introduced in Sec. IV B. Because the coupling is essential at angles η close to $\pi/2$, we focus on $\eta = \pi/2$, i.e. the direction of the magnetic field perpendicular to the separation between the nodes. The coupling Δ for a particular form of the function $m(k_z)$ has been computed microscopically in Ref. 32. Here, we generalise this derivation to the case of a generic function $m(k_z)$.

Following Ref. 32, we perform a unitary rotation

$$\psi \rightarrow \phi = e^{i\frac{\pi}{2}\hat{\sigma}_y} \psi \quad (\text{C1})$$

in the pseudospin space and rewrite the equation $\hat{\mathcal{H}}^2 \psi = E^2 \psi$ for a disorder-free system in the form

$$\left[-v_F^2 \partial_y^2 + v_F^2 k_x^2 + m^2 \left(k_z + \frac{e}{c} B y \right) - E^2 \right] \phi = B m' \left(k_z + \frac{e}{c} B y \right) \sigma_z \phi. \quad (\text{C2})$$

We emphasise that near the node $\chi = -1$ the rotation (C1) of the basis in the pseudospin space is distinct from that described by Eq. (4.4), which we used in Section IV in order to obtain the quasiparticle wavefunctions in the absence of the internodal coupling. Whereas the transformation (4.4) is different near different nodes, the rotation (C1) is a global transformation of the basis; the two transformations match near the node with $\chi = +1$ in the case $\eta = \pi/2$ under consideration. In this section, we use also the coordinate frame described by Eqs. (4.2) and (4.3) and shown in Fig. 3 for $\eta = \pi/2$, i.e. with $k_{z'} = k_x$, $k_{x'} = -k_z$.

Equation (C2) is similar to the Schrödinger equation of a quadratically dispersive particle in a double-well potential⁵⁴. The tunnelling amplitude between the two wells may be computed in the quasiclassical approximation. To that end, we introduce the classical (complex) momentum along the y axis

$$k_y(y) = \left[m^2 \left(k_z + \frac{e}{c} B y \right) + v_F^2 k_x^2 - E^2 \right]^{\frac{1}{2}}. \quad (\text{C3})$$

The quasiclassical solutions of Eq. (C2) in the region between the minima of the wells, where the amplitude of the wavefunction is small, are given by

$$\phi_{1,2} = \sum_{\pm} C_{1,2}^{(\pm)} e^{\pm \int_{y^*}^y k_y dy \pm \int_{y^*}^y \frac{dy e B m'}{2 c k_y}}, \quad (\text{C4})$$

where $C_1^{(\pm)}$ and $C_2^{(\pm)}$ are constants and the coordinate y^* may be chosen arbitrarily. Between the nodes, the function m , which characterises the bandwidth of the quasiparticles, is large compared to the all the other momentum scales of low-energy quasiparticles. Therefore, in the region of applicability of Eq. (C4) it is possible to make the approximation

$k_y \approx m$. Substituting the solutions (C4) for the wavefunctions between the nodes into the Schrödinger equation $\hat{H}\psi = E\psi$ with the Hamiltonian (3.1) in the absence of the impurity potential, we obtain the relations

$$C_2^{(\pm)} = \left[\frac{(E \mp v_F k_x)}{2m(y^*)} \right]^{\pm 1} C_1^{(\pm)} \quad (\text{C5})$$

between the coefficients $C_1^{(\pm)}$ and $C_2^{(\pm)}$.

Equation (C4) describes the wavefunction between the nodes, where the exponential is small. Solving the Schrödinger equation $\hat{H}\psi = E\psi$, with the function m linearised according to Eq. (4.1), gives the (non-normalised) wavefunction near a node of chirality χ in the form

$$\begin{aligned} \begin{pmatrix} \phi_1 \\ \phi_2 \end{pmatrix} &= \cos \left[\frac{\pi c(E^2 - v_F^2 k_x^2)}{2v_F^2 eB} \right] e^{-\frac{c(Q + \chi k_z + \chi \frac{eBy}{c})^2}{2|e|B}} \left(Q + \chi k_z - \chi \frac{eBy}{c} \right)^{\frac{c(E^2 - v_F^2 k_x^2)}{2v_F^2 |e|B}} \begin{pmatrix} 1 \\ \frac{E - \chi k_x c}{2\chi(Qc + \chi k_x c - \chi By)} \end{pmatrix} \\ &+ \frac{\sqrt{2\pi}}{\Gamma \left[\frac{c(E^2 - v_F^2 k_x^2)}{2v_F^2 eB} \right]} \left(\frac{|e|B}{2c} \right)^{\frac{c(E^2 - v_F^2 k_x^2)}{2v_F^2 |e|B} + \frac{1}{2}} e^{\frac{c(Q + \chi k_z + \chi \frac{eBy}{c})^2}{2|e|B}} \left(Q + \chi k_z - \chi \frac{eBy}{c} \right)^{\frac{c(E^2 - v_F^2 k_x^2)}{2v_F^2 |e|B} - 1} \begin{pmatrix} 1 \\ \frac{2\chi(Qc + \chi k_x c - \chi By)}{E + \chi k_x} \end{pmatrix}, \end{aligned} \quad (\text{C6})$$

where ϕ_1 and ϕ_2 are the components of the wavefunction ϕ with pseudospins, respectively, parallel and antiparallel to the x axis. The exponent $\frac{c(Q + \chi k_z + \chi \frac{eBy}{c})^2}{2|e|B} \equiv l_B^2 \left(\chi Q + \frac{eBy}{c} - k_x \right)^2$ in Eq. (C6) is small near the node of chirality χ , in agreement with the discussion in Sec. IV A 1. As Eq. (C6) applies in the vicinity of the node, where the function m may be linearised, it contains both factors contributions exponentially decaying and exponentially increasing away from the node.

Matching the asymptotics of Eq. (C6) at large values of the quantity $Q + \chi k_z + \chi \frac{eBy}{c}$ with the solution (C4) between the nodes and obtaining the values of the coefficients C_1 and C_2 , we arrive at the values of the quasiparticle energies in the form

$$\frac{(E^2 - v_F^2 k_x^2)c}{2|e|Bv_F^2} = \frac{1}{2\pi} e^{-\frac{2c}{|e|Bv_F} \int_{-Q}^Q m(p_z) dp_z}, \quad (\text{C7})$$

which leads to the value of the internodal coupling Δ given by Eq. (4.15) in the main text.

Weakly hybridised states

At $\eta = \pi/2$, the dispersion of the quasiparticles at decoupled nodes is given by $E = \chi v_F k_x$, as follows from Eq. (4.10). The internodal coupling leads to the hybridisation of quasiparticle states at different nodes and the modification of the dispersion. As discussed in Sec. IV B, the states at $\eta = \pi/2$ get hybridised most strongly for small momenta k_x .

As we discuss also in Sec. VI, the chemical potential μ in realistic WSMs corresponds to large momenta, $|k_x| \gg \Delta/v_F$, at which the states are weakly hybridised by the internodal tunnelling. Despite being weak, taking into account this hybridisation is essential for obtaining a finite conductivity in the case of the angle η being close to $\pi/2$ we consider.

In the regime under consideration, a state with a positive momentum k_x and energy $E \approx v_F k_x + \frac{\Delta^2}{2v_F k_x}$ [cf. Eq. (4.14)] at the node $\chi = +1$ acquires, due to hybridisation, a small correction from the other node, $\chi = -1$. The wavefunction of such a state is given by

$$\begin{aligned} |\phi_{+1\mathbf{k}}\rangle &= \left(\frac{|e|B}{\pi c} \right)^{1/4} e^{-\frac{c(Q + k_z + \frac{eBy}{c})^2}{2|e|B}} \begin{pmatrix} 1 \\ 0 \end{pmatrix} \\ &- \sqrt{\frac{E - v_F k_x}{E + v_F k_x}} \left\{ \left(\frac{|e|B}{\pi c} \right)^{1/4} e^{-\frac{c(Q - k_z - \frac{eBy}{c})^2}{2|e|B}} \begin{pmatrix} \frac{E + v_F k_x}{2m} \\ 1 \end{pmatrix} - \left(\frac{\pi c}{|e|B} \right)^{1/4} \left(\frac{E}{v_F} + k_x \right) e^{\frac{c(Q - k_z - \frac{eBy}{c})^2}{2|e|B}} \begin{pmatrix} 1 \\ 0 \end{pmatrix} \right\}. \end{aligned} \quad (\text{C8})$$

The first term in the right-hand side of Eq. (C8) describes the wavefunction of the quasiparticle at node $\chi = 1$. This term is peaked at $k_z = -Q - \frac{eBy}{c}$, i.e. at the location of the first node in the xz plane in momentum space, as

discussed in Sec. (IV A 1). The last two terms in Eq. (C8) describe the small correction due to the presence of the other node, with the chirality $\chi = -1$. Those terms are peaked at $k_z = Q - \frac{eBy}{c}$ and are suppressed by the small prefactor $\sqrt{\frac{E - v_F k_x}{E + v_F k_x}} \approx \frac{\Delta}{v k_x \sqrt{2}}$ in the limit of large momenta $k_x \gg \Delta/v_F$ under consideration.

Similarly, the state at the node with chirality $\chi = -1$ is weakly hybridised, due to the internodal tunnelling, with the other node whose chirality is $\chi = -1$. The wavefunction of this state is given by

$$|\phi_{-1\mathbf{k}}\rangle = \left(\frac{|e|B}{\pi c}\right)^{1/4} e^{-\frac{c(Q - k_z - \frac{eBy}{c})^2}{2|e|B}} \begin{pmatrix} 0 \\ 1 \end{pmatrix} - \sqrt{\frac{E + v_F k_x}{E - v_F k_x}} \left\{ \left(\frac{|e|B}{\pi c}\right)^{1/4} e^{-\frac{c(Q + k_z + \frac{eBy}{c})^2}{2|e|B}} \begin{pmatrix} 1 \\ \frac{E - v_F k_x}{2m} \end{pmatrix} - \left(\frac{\pi c}{|e|B}\right)^{1/4} \left(\frac{E}{v_F} - k_x\right) e^{\frac{c(Q + k_z + \frac{eBy}{c})^2}{2|e|B}} \begin{pmatrix} 0 \\ 1 \end{pmatrix} \right\}. \quad (\text{C9})$$

The energy of this state is given by $E \approx -v_F k_x - \frac{\Delta^2}{2v_F k_x}$ for the large momenta k_x under consideration. The first and the last two terms in Eq. (C9) describe, respectively, the state of a particle at the node with chirality $\chi = -1$ and a correction due to the presence of the other node.

Appendix D: Internodal scattering rate away from $\eta = \pi/2$

In this section, we present details of the calculation of the internodal scattering rate (5.3) for angles η away from $\pi/2$, where the effect of coherent internodal tunnelling on the quasiparticle dispersion and scattering may be neglected. For simplicity, we assume that the system is rectangular, with the edges parallel to the x' , y and z' axes.

As discussed in Sec. V, the scattering rate is determined by the matrix element of scattering of a quasiparticle near node χ with momentum $\mathbf{p} = (\mathbf{p}_{x'}, \mathbf{p}_{z'})$ in the $x'z'$ plane into the state with momentum $\mathbf{k} = (\mathbf{k}_{x'}, \mathbf{k}_{z'})$ near node χ' on the potential $u(\mathbf{r} - \mathbf{R}_i)$ of the i -th impurity, with the location $\mathbf{R}_i = (R_x^{(i)}, R_y^{(i)}, R_z^{(i)})$, is given by

$$\langle \psi_{\chi\mathbf{p}} | u(\mathbf{r} - \mathbf{R}_i) | \psi_{\chi'\mathbf{k}} \rangle \equiv \int d\mathbf{r} \psi_{\chi\mathbf{p}}^\dagger(\mathbf{r}) u(\mathbf{r} - \mathbf{R}_i) \psi_{\chi'\mathbf{k}}(\mathbf{r}) = \frac{4\pi Z_i e^2}{V\varepsilon} \int d\mathbf{r} \psi_{\chi}^\dagger(\mathbf{r}) \psi_{\chi'}(\mathbf{r}) \sum_{\mathbf{q}} \frac{e^{i\mathbf{q}(\mathbf{r} - \mathbf{R}_i)}}{q^2 + \varkappa^2}, \quad (\text{D1})$$

where $\psi_{\chi\mathbf{p}}(\mathbf{r})$ and $\psi_{\chi'\mathbf{k}}(\mathbf{r})$ are the wavefunctions of the respective states, given by Eq. (4.9). In Eq. (D1) we used the Fourier transform $u(\mathbf{q}) = \frac{4\pi Z_i e^2}{q^2 + \varkappa^2}$ of the potential⁴⁷ of an impurity.

The conductivity is determined by internodal scattering, with $\chi = -\chi'$, while intranodal scattering, corresponding to $\chi = \chi'$, has no effect on transport since it does not change the quasiparticle velocity. Using Eq. (4.9) for the states with $\chi = 1$ and $\chi' = -1$ gives the matrix element for internodal scattering in the form

$$\langle \psi_{+1\mathbf{p}} | u(\mathbf{r} - \mathbf{R}_i) | \psi_{-1\mathbf{k}} \rangle = \frac{4\pi Z_i e^2 \cos \eta}{V\varepsilon} \sum_{q_y} \exp \left[-\frac{c(p_{x'} - k_{x'} - 2Q \sin \eta)^2}{4|e|B} - \frac{cq_y^2}{4|e|B} + \frac{icq_y}{eB} \left(\frac{p_{x'} + k_{x'}}{2} - \frac{eBR_y^{(i)}}{c} \right) \right] \frac{e^{-i(p_{x'} - k_{x'})R_{x'}^{(i)} - i(p_{z'} - k_{z'})R_{z'}^{(i)}}}{q_y^2 + (p_{x'} - k_{x'})^2 + (p_{z'} - k_{z'})^2 + \varkappa^2}. \quad (\text{D2})$$

Performing disorder averaging, $\langle \dots \rangle_{\text{dis}} = \frac{1}{V} \int \dots d\mathbf{R}_i$, of the square of the matrix element over the location of the impurity gives

$$\left\langle \left| \langle \psi_{+1\mathbf{p}} | U | \psi_{-1\mathbf{k}} \rangle \right|^2 \right\rangle_{\text{dis}} = N \left(\frac{4\pi e^2 \cos \eta}{V\varepsilon} \right)^2 e^{-\frac{c(p_{x'} - k_{x'} - 2Q \sin \eta)^2}{2|e|B}} \sum_{q_y} \frac{e^{-\frac{cq_y^2}{2|e|B}}}{[q_y^2 + (p_{x'} - k_{x'})^2 + (p_{z'} - k_{z'})^2 + \varkappa^2]^2}, \quad (\text{D3})$$

where N is the number of impurities in the system.

The expression in the denominator in Eq. (D3) may be approximated as

$$q_y^2 + (p_{x'} - k_{x'})^2 + (p_{z'} - k_{z'})^2 + \varkappa^2 \approx (2Q)^2. \quad (\text{D4})$$

Indeed, the sum with respect to q_y in Eq. (D3) is dominated by momenta q_y on the order of the inverse magnetic length l_B^{-1} , which is given by Eq. (3.4) and is significantly smaller than the separation $2Q$ between the nodes. The

inverse screening length \varkappa is on the order of $\alpha^{\frac{1}{2}}/l_B$ and is also significantly exceeded by the momentum Q . Because the energies of the quasiparticles are small compared to the bandwidth and according to Eq. (4.10), $p_{z'} \approx -Q \cos \eta$ and $k_{z'} \approx Q \cos \eta$. The dynamics of the quasiparticles correspond to the range of momenta where the function m in the Hamiltonian (3.1) may be linearised, Eq. (4.1). Together with Eqs. (4.2) and (4.3) this gives $k_{x'} \approx Q \sin \eta$ and $p_{x'} \approx -Q \sin \eta$. Taking into account the values of all momenta and neglecting all momentum scales smaller than Q , we arrive at the approximation (D4).

Performing the integration with respect to momentum q_y (with the replacement $\sum_{q_y} \rightarrow L_y \int \frac{dq_y}{2\pi}$) and utilising Eq. D3 gives

$$\left\langle |\langle \psi_{+1\mathbf{p}} | U | \psi_{-1\mathbf{k}} \rangle|^2 \right\rangle_{\text{dis}} \approx N \left(\frac{4\pi e^2 \cos \eta}{V\varepsilon} \right)^2 e^{-\frac{c(p_{x'} - k_{x'} - 2Q \sin \eta)^2}{2|e|B}} \frac{L_y}{2\pi} \sqrt{\frac{2|e|B\pi}{c}} \frac{1}{[4Q^2]^2}. \quad (\text{D5})$$

Substituting the disorder-averaged scattering element (D5) into the expression (5.1) and performing integration over the momentum components $k_{x'}$ and $k_{z'}$, we arrive at the expression (5.3) for the internodal scattering rate.

Appendix E: Internodal scattering rate at $\eta = \pi/2$

In this section, we provide the details of the calculation of the quasiparticle scattering rate $1/\tau$ at $\eta = \pi/2$, i.e. for the magnetic field perpendicular to the separation between the nodes. The resistivity at this angle is determined by the processes of scattering between states $|\phi_{+1\mathbf{p}}\rangle$ and $|\phi_{-1\mathbf{k}}\rangle$, given, respectively, by Eqs. (C8) and (C9). The scattering rate between such states is given by

$$\frac{1}{\tau} = 2\pi \int \left\langle |\langle \phi_{+1\mathbf{p}} | U | \phi_{-1\mathbf{k}} \rangle|^2 \right\rangle_{\text{dis}} \delta(E_{+1\mathbf{p}} - E_{-1\mathbf{k}}) \frac{S_{xz} d\mathbf{p}}{(2\pi)^2}, \quad (\text{E1})$$

where $E_{+1\mathbf{p}}$ and $E_{-1\mathbf{k}}$ are, respectively, the energies of the states $|\phi_{+1\mathbf{p}}\rangle$ and $|\phi_{-1\mathbf{k}}\rangle$ and S_{xz} is the cross-section area of the system in the xz plane.

Similarly to the case of internodal scattering at angles η away from $\pi/2$, the scattering rate $1/\tau$ is determined by the matrix element $\langle \phi_{+1\mathbf{p}} | u(\mathbf{r} - \mathbf{R}_i) | \phi_{-1\mathbf{k}} \rangle$ of scattering off an impurity at location \mathbf{R}_i . Noticing that the exponentials in Eqs. (C8) and (C9) which grow away from the nodes do not contribute to this matrix elements, we obtain

$$\begin{aligned} & \langle \phi_{+1\mathbf{p}} | u(\mathbf{r} - \mathbf{R}_i) | \phi_{-1\mathbf{k}} \rangle = \\ & - e^{-\frac{c(p_z - k_z)^2}{4|e|B}} \sqrt{\frac{E_{-1\mathbf{k}} + v_F k_x}{E_{-1\mathbf{k}} - v_F k_x}} \frac{4\pi Z_i e^2}{V\varepsilon} \sum_{q_y} \frac{e^{-\frac{cq_y^2}{4|e|B} - \frac{icq_y}{2eB}(2Q + p_z + k_z) - iq_y R_y^{(i)} - i(p_x - k_x)R_x^{(i)} - i(p_z - k_z)R_z^{(i)}}}{q_y^2 + (p_x - k_x)^2 + (p_z - k_z)^2 + \varkappa^2} \\ & - e^{-\frac{c(p_z - k_z)^2}{4|e|B}} \sqrt{\frac{E_{+1\mathbf{p}} - v_F p_x}{E_{+1\mathbf{p}} + v_F p_x}} \frac{4\pi Z_i e^2}{V\varepsilon} \sum_{q_y} \frac{e^{-\frac{cq_y^2}{4|e|B} - \frac{icq_y}{2eB}(-2Q + p_z + k_z) - iq_y R_y^{(i)} - i(p_x - k_x)R_x^{(i)} - i(p_z - k_z)R_z^{(i)}}}{q_y^2 + (p_x - k_x)^2 + (p_z - k_z)^2 + \varkappa^2}, \quad (\text{E2}) \end{aligned}$$

The first and the second lines in Eq. (E2) come from the wavefunctions near nodes $\chi = -1$ and $\chi = +1$.

The matrix element of scattering off the total potential $U(\mathbf{r}) = \sum_i u(\mathbf{r} - \mathbf{R}_i)$, averaged over the realisations of the potential, is given by

$$\begin{aligned} \langle |\langle \phi_{+1\mathbf{p}} | U | \phi_{-1\mathbf{k}} \rangle|^2 \rangle_{\text{dis}} &= \frac{N}{V} \langle |\langle \phi_{+1\mathbf{p}} | u(\mathbf{r} - \mathbf{R}_i) | \phi_{-1\mathbf{k}} \rangle|^2 \rangle_{\text{dis}} \\ &= N \left(\frac{4\pi e^2}{V\varepsilon} \right)^2 \frac{L_y}{2\pi} \left\{ \left(\frac{E_{-1\mathbf{k}} + v_F k_x}{E_{-1\mathbf{k}} - v_F k_x} + \frac{E_{+1\mathbf{p}} - v_F p_x}{E_{+1\mathbf{p}} + v_F p_x} \right) \int \frac{dq_y e^{-\frac{c(p_z - k_z)^2}{2|e|B} - \frac{cq_y^2}{2|e|B}}}{[q_y^2 + (p_x - k_x)^2 + (p_z - k_z)^2 + \varkappa^2]^2} \right. \\ & \quad \left. + \sqrt{\frac{(E_{-1\mathbf{k}} + v_F k_x)(E_{+1\mathbf{p}} - v_F p_x)}{(E_{-1\mathbf{k}} - v_F k_x)(E_{+1\mathbf{p}} + v_F p_x)}} \int \frac{dq_y e^{-\frac{c(p_z - k_z)^2}{2|e|B} - \frac{cq_y^2}{2|e|B}} \left(e^{\frac{2iQc q_y}{eB}} + e^{-\frac{2iQc q_y}{eB}} \right)}{[q_y^2 + (p_x - k_x)^2 + (p_z - k_z)^2 + \varkappa^2]^2} \right\}. \quad (\text{E3}) \end{aligned}$$

The quantities $[q_y^2 + (p_x - k_x)^2 + (p_z - k_z)^2 + \varkappa^2]^{\frac{1}{2}}$ in Eq. (E3) have the meaning of the effective momentum change of a plane-wave state scattered off the potential. We emphasise, however, that, unlike the case of internodal scattering considered in Appendix E, this differences cannot be approximated by the separation $2Q$ between the Weyl nodes.

To compute the scattering time (E1), we perform first the integration of the expression (E3) with respect to the momentum p_z . The first line gives a contribution proportional to

$$\int \frac{dp_z dq_y e^{-\frac{c(p_z - k_z)^2}{2|e|B} - \frac{cq_y^2}{2|e|B}}}{[q_y^2 + (p_x - k_x)^2 + (p_z - k_z)^2 + \varkappa^2]^2} = \frac{\pi}{(p_x - k_x)^2 + \varkappa^2} - \frac{\pi c}{2|e|B} e^{\frac{c(p_x - k_x)^2}{2|e|B} + \frac{c\varkappa^2}{2|e|B}} E_1 \left[\frac{c(p_x - k_x)^2}{2|e|B} + \frac{c\varkappa^2}{2|e|B} \right], \quad (\text{E4})$$

where $E_1(x) = \int_1^\infty dt e^{-tx}/t$ is the exponential integral. The characteristic momentum difference $p_x - k_x$ is on the order of $|\mu|/v_F$, with μ being the chemical potential, and in the limit of strong magnetic fields under consideration (the ‘‘ultraquantum’’ limit) is exceeded by the inverse magnetic length $l_B^{-1} = \sqrt{|e|B}/c$. As a result, and considering also the smallness of the magnetic length l_B in comparison with the screening length \varkappa , the second term in the right-hand side part of Eq. (E4) may be neglected and we may approximate

$$\int \frac{dp_z dq_y e^{-\frac{c(p_z - k_z)^2}{2|e|B} - \frac{cq_y^2}{2|e|B}}}{[q_y^2 + (p_x - k_x)^2 + (p_z - k_z)^2 + \varkappa^2]^2} \approx \frac{\pi}{(p_x - k_x)^2 + \varkappa^2}. \quad (\text{E5})$$

The integral of the second line of Eq. (E3) with respect to the momentum p_z may be represented in the form

$$\int \frac{dp_z dq_y e^{-\frac{c(p_z - k_z)^2}{2|e|B} - \frac{cq_y^2}{2|e|B}} \left(e^{\frac{2iQcq_y}{eB}} + e^{-\frac{2iQcq_y}{eB}} \right)}{[q_y^2 + (p_x - k_x)^2 + (p_z - k_z)^2 + \varkappa^2]^2} = \frac{2\pi I \left[l_B Q, l_B \sqrt{(p_x - k_x)^2 + \varkappa^2} \right]}{(p_x - k_x)^2 + \varkappa^2}, \quad (\text{E6})$$

where the magnetic length l_B is given by Eq. (3.4) and the integral $I(s, t)$ is given by Eq. (6.3). Performing integration with respect to p_z in the expression (E1) for the scattering rate and utilising Eqs. (E4), (E5) and (E6), we arrive at the scattering rate given by Eqs. (6.2) and (6.3).

In the main text we consider the ranges of parameters that correspond to two limiting cases in the integral $I(s, t)$,

$$I(s, t) = \frac{t^2}{\pi} \int \frac{\cos(2sy) e^{-\frac{z^2 + y^2}{2}}}{(y^2 + z^2 + t^2)^2} dz dy \rightarrow \begin{cases} 1, & st \ll 1, \\ 0, & st \gg 1. \end{cases} \quad (\text{E7})$$

-
- ¹ Xiangang Wan, Ari M. Turner, Ashvin Vishwanath, and Sergey Y. Savrasov, ‘‘Topological semimetal and Fermi-arc surface states in the electronic structure of pyrochlore iridates,’’ *Phys. Rev. B* **83**, 205101 (2011).
- ² Su-Yang Xu, Ilya Belopolski, Daniel S. Sanchez, Chenglong Zhang, Guoqing Chang, Cheng Guo, Guang Bian, Zhujun Yuan, Hong Lu, Tay-Rong Chang, Pavel P. Shibayev, Mykhailo L. Prokopovych, Nasser Alidoust, Hao Zheng, Chi-Cheng Lee, Shin-Ming Huang, Raman Sankar, Fangcheng Chou, Chuang-Han Hsu, Horng-Tay Jeng, Arun Bansil, Titus Neupert, Vladimir N. Strocov, Hsin Lin, Shuang Jia, and M. Zahid Hasan, ‘‘Experimental discovery of a topological Weyl semimetal state in TaP,’’ *Science Advances* **1** (2015), 10.1126/sciadv.1501092.
- ³ B. Q. Lv, H. M. Weng, B. B. Fu, X. P. Wang, H. Miao, J. Ma, P. Richard, X. C. Huang, L. X. Zhao, G. F. Chen, Z. Fang, X. Dai, T. Qian, and H. Ding, ‘‘Experimental discovery of Weyl semimetal TaAs,’’ *Phys. Rev. X* **5**, 031013 (2015).
- ⁴ M. Zahid Hasan, Su-Yang Xu, Ilya Belopolski, and Shin-Ming Huang, ‘‘Discovery of Weyl fermion semimetals and topological Fermi arc states,’’ *Annual Review of Condensed Matter Physics* **8**, 289–309 (2017), <https://doi.org/10.1146/annurev-conmatphys-031016-025225>.
- ⁵ N. P. Armitage, E. J. Mele, and Ashvin Vishwanath, ‘‘Weyl and Dirac semimetals in three-dimensional solids,’’ *Rev. Mod. Phys.* **90**, 015001 (2018).
- ⁶ Oskar Vafek and Ashvin Vishwanath, ‘‘Dirac fermions in solids: From high- T_c cuprates and graphene to topological insulators and Weyl semimetals,’’ *Annual Review of Condensed Matter Physics* **5**, 83–112 (2014).
- ⁷ A. A. Burkov, ‘‘Weyl metals,’’ *Annual Review of Condensed Matter Physics* **9**, 359–378 (2018).
- ⁸ A A Burkov, ‘‘Chiral anomaly and transport in Weyl metals,’’ *Journal of Physics: Condensed Matter* **27**, 113201 (2015).
- ⁹ D. T. Son and B. Z. Spivak, ‘‘Chiral anomaly and classical negative magnetoresistance of Weyl metals,’’ *Phys. Rev. B* **88**, 104412 (2013).
- ¹⁰ H. B. Nielsen and M. Ninomiya, ‘‘Absence of neutrinos on a lattice: (i). proof by homotopy theory,’’ *Nucl. Phys. B* **185**, 20 – 40 (1981).
- ¹¹ Dmitri E. Kharzeev and Ho-Ung Yee, ‘‘Anomaly induced chiral magnetic current in a Weyl semimetal: Chiral electronics,’’ *Phys. Rev. B* **88**, 115119 (2013).
- ¹² Xiaochun Huang, Lingxiao Zhao, Yujia Long, Peipei Wang, Dong Chen, Zhanhai Yang, Hui Liang, Mianqi Xue, Hongming Weng, Zhong Fang, Xi Dai, and Genfu Chen, ‘‘Observation of the Chiral-Anomaly-Induced Negative Magne-

- toresistance in 3D Weyl Semimetal TaAs,” *Phys. Rev. X* **5**, 031023 (2015).
- 13 Cheng-Long Zhang, Su-Yang Xu, Ilya Belopolski, Zhujun Yuan, Ziquan Lin, Bingbing Tong, Guang Bian, Nasser Alidoust, Chi-Cheng Lee, Shin-Ming Huang, Tay-Rong Chang, Guoqing Chang, Chuang-Han Hsu, Horng-Tay Jeng, Madhab Neupane, Daniel S. Sanchez, Hao Zheng, Junfeng Wang, Hsin Lin, Chi Zhang, Hai-Zhou Lu, Shun-Qing Shen, Titus Neupert, M. Zahid Hasan, and Shuang Jia, “Signatures of the Adler-Bell-Jackiw anomaly in a Weyl fermion semimetal,” *Nature Communications* **7**, 10735 (2016).
 - 14 X. Yang, Y. Liu, Z. Wang, Y. Zheng, and Z.-a. Xu, “Chiral anomaly induced negative magnetoresistance in topological Weyl semimetal NbAs,” *ArXiv e-prints* (2015), arXiv:1506.03190 [cond-mat.mtrl-sci].
 - 15 JianHua Du, HangDong Wang, Qin Chen, QianHui Mao, Rajwali Khan, BinJie Xu, YuXing Zhou, YanNan Zhang, JinHu Yang, Bin Chen, ChunMu Feng, and MingHu Fang, “Large unsaturated positive and negative magnetoresistance in Weyl semimetal TaP,” *Science China Physics, Mechanics & Astronomy* **59**, 657406 (2016).
 - 16 Zhen Wang, Yi Zheng, Zhixuan Shen, Yunhao Lu, Hanyan Fang, Feng Sheng, Yi Zhou, Xiaojun Yang, Yupeng Li, Chunmu Feng, and Zhu-An Xu, “Helicity-protected ultrahigh mobility Weyl fermions in NbP,” *Phys. Rev. B* **93**, 121112 (2016).
 - 17 S. Jia, S.-Y. Xu, and M. Z. Hasan, “Weyl semimetals, Fermi arcs and chiral anomalies,” *Nature Materials* **15**, 1140–1144 (2016), arXiv:1612.00416 [cond-mat.mes-hall].
 - 18 Jun Xiong, Satya K. Kushwaha, Tian Liang, Jason W. Krizan, Max Hirschberger, Wudi Wang, R. J. Cava, and N. P. Ong, “Evidence for the chiral anomaly in the Dirac semimetal Na₃Bi,” *Science* **350**, 413–416 (2015).
 - 19 Max Hirschberger, Satya Kushwaha, Zhijun Wang, Quinn Gibson, Sihang Liang, Carina A. Belvin, B. A. Bernevig, R. J. Cava, and N. P. Ong, “The chiral anomaly and thermopower of Weyl fermions in the half-Heusler GdPtBi,” *Nature Materials* **15**, 1161 EP – (2016).
 - 20 Sihang Liang, Jingjing Lin, Satya Kushwaha, Jie Xing, Ni Ni, R. J. Cava, and N. P. Ong, “Experimental tests of the chiral anomaly magnetoresistance in the Dirac-Weyl semimetals Na₃Bi and GdPtBi,” *Phys. Rev. X* **8**, 031002 (2018).
 - 21 Philip J. W. Moll, Nityan L. Nair, Toni Helm, Andrew C. Potter, Itamar Kimchi, Ashvin Vishwanath, and James G. Analytis, “Transport evidence for Fermi-arc-mediated chirality transfer in the Dirac semimetal Cd₃As₂,” *Nature* **535**, 266 (2016).
 - 22 Andrew C. Potter, Itamar Kimchi, and Ashvin Vishwanath, “Quantum oscillations from surface Fermi arcs in Weyl and Dirac semimetals,” *Nature Communications* **5**, 5161 (2014).
 - 23 S. V. Syzranov, Ya. I. Rodionov, and B. Skinner, “Adiabatic dechiralization and thermodynamics of Weyl semimetals,” *Phys. Rev. B* **98**, 081114 (2018).
 - 24 E. V. Gorbar, V. A. Miransky, I. A. Shovkovy, and P. O. Sukhachov, “Consistent hydrodynamic theory of chiral electrons in Weyl semimetals,” *Phys. Rev. B* **97**, 121105 (2018).
 - 25 E. V. Gorbar, V. A. Miransky, I. A. Shovkovy, and P. O. Sukhachov, “Hydrodynamic electron flow in a Weyl semimetal slab: Role of Chern-Simons terms,” *Phys. Rev. B* **97**, 205119 (2018).
 - 26 Andrew Lucas, Richard A. Davison, and Subir Sachdev, “Hydrodynamic theory of thermoelectric transport and negative magnetoresistance in Weyl semimetals,” *Proceedings of the National Academy of Sciences* **113**, 9463–9468 (2016), <https://www.pnas.org/content/113/34/9463.full.pdf>.
 - 27 Naoki Yamamoto, “Chiral transport of neutrinos in supernovae: Neutrino-induced fluid helicity and helical plasma instability,” *Phys. Rev. D* **93**, 065017 (2016).
 - 28 Victor Galitski, Mehdi Kargarian, and Sergey Syzranov, “Dynamo effect and turbulence in hydrodynamic Weyl metals,” *Phys. Rev. Lett.* **121**, 176603 (2018).
 - 29 E. V. Gorbar, V. A. Miransky, I. A. Shovkovy, and P. O. Sukhachov, “Nonlocal transport in Weyl semimetals in the hydrodynamic regime,” *Phys. Rev. B* **98**, 035121 (2018).
 - 30 P. O. Sukhachov, E. V. Gorbar, I. A. Shovkovy, and V. A. Miransky, “Collective excitations in Weyl semimetals in the hydrodynamic regime,” *Journal of Physics: Condensed Matter* **30**, 275601 (2018).
 - 31 J. Gooth, F. Menges, N. Kumar, V. Suß, C. Shekhar, Y. Sun, U. Drechsler, R. Zierold, C. Felser, and B. Gotsmann, “Thermal and electrical signatures of a hydrodynamic electron fluid in tungsten diphosphide,” *Nature Communications* **9**, 4093 (2018).
 - 32 D. R. Saykin, K. S. Tikhonov, and Ya. I. Rodionov, “Landau levels with magnetic tunneling in a Weyl semimetal and magnetoconductance of a ballistic p - n junction,” *Phys. Rev. B* **97**, 041202 (2018).
 - 33 Ching-Kit Chan and Patrick A. Lee, “Emergence of gapped bulk and metallic side walls in the zeroth Landau level in Dirac and Weyl semimetals,” *Phys. Rev. B* **96**, 195143 (2017).
 - 34 Ming-Chien Hsu, Hsin Lin, M. Zahid Hasan, and Shin-Ming Huang, “Topologically distinct Weyl-fermion pairs: on the effect of magnetic tunnelling,” *arXiv e-prints*, arXiv:1903.07484 (2019), arXiv:1903.07484 [cond-mat.mes-hall].
 - 35 Yuxuan Jiang, Zhiling Dun, Seongphil Moon, Haidong Zhou, Mikito Koshino, Dmitry Smirnov, and Zhigang Jiang, “Landau quantization in coupled Weyl points: A case study of semimetal NbP,” *Nano Letters* **18**, 7726–7731 (2018), pMID: 30403143, <https://doi.org/10.1021/acs.nanolett.8b03418>.
 - 36 Cheng-Long Zhang, Su-Yang Xu, C. M. Wang, Ziquan Lin, Z. Z. Du, Cheng Guo, Chi-Cheng Lee, Hong Lu, Yiyang Feng, Shin-Ming Huang, Guoqing Chang, Chuang-Han Hsu, Haiwen Liu, Hsin Lin, Liang Li, Chi Zhang, Jinglei Zhang, Xin-Cheng Xie, Titus Neupert, M. Zahid Hasan, Hai-Zhou Lu, Junfeng Wang, and Shuang Jia, “Magnetic-tunnelling-induced Weyl node annihilation in TaP,” *Nature Physics* **13**, 979–986 (2017).
 - 37 Pallab Goswami, J. H. Pixley, and S. Das Sarma, “Axial anomaly and longitudinal magnetoresistance of a generic three-dimensional metal,” *Phys. Rev. B* **92**, 075205 (2015).
 - 38 Jan Behrends, Roni Ilan, and Jens H. Bardarson, “Anomalous conductance scaling in strained Weyl semimetals,” *arXiv e-prints*, arXiv:1906.08277 (2019), arXiv:1906.08277 [cond-mat.mes-hall].
 - 39 Xiao Xiao, K. T. Law, and P. A. Lee, “Magnetoconductivity in Weyl semimetals: Effect of chemical potential and temperature,” *Phys. Rev. B* **96**, 165101 (2017).
 - 40 R. D. dos Reis, M. O. Ajeesh, N. Kumar, F. Arnold, C. Shekhar, M. Naumann, M. Schmidt, M. Nicklas, and E. Hassinger, “On the search for the chiral anomaly in Weyl semimetals:

- the negative longitudinal magnetoresistance,” *New Journal of Physics* **18**, 085006 (2016).
- ⁴¹ J.-P. Jay-Gerin, M.J. Aubin, and L.G. Caron, “The electron mobility and the static dielectric constant of Cd_3As_2 at 4.2 K,” *Solid State Communications* **21**, 771 – 774 (1977).
- ⁴² O. Madelung, U. Rössler, and M. Schulz, eds., “Cadmium arsenide (Cd_3As_2) optical properties, dielectric constants,” in *Non-Tetrahedrally Bonded Elements and Binary Compounds I* (Springer Berlin Heidelberg, Berlin, Heidelberg, 1998) pp. 1–10.
- ⁴³ G. S. Jenkins, C. Lane, B. Barbiellini, A. B. Sushkov, R. L. Carey, Fengguang Liu, J. W. Krizan, S. K. Kushwaha, Q. Gibson, Tay-Rong Chang, Horng-Tay Jeng, Hsin Lin, R. J. Cava, A. Bansil, and H. D. Drew, “Three-dimensional Dirac cone carrier dynamics in Na_3Bi and Cd_3As_2 ,” *Phys. Rev. B* **94**, 085121 (2016).
- ⁴⁴ J. Buckeridge, D. Jevdokimovs, C. R. A. Catlow, and A. A. Sokol, “Bulk electronic, elastic, structural, and dielectric properties of the Weyl semimetal TaAs,” *Phys. Rev. B* **93**, 125205 (2016).
- ⁴⁵ The value of the chirality assigned to each node here matches the flux $\chi = \frac{i}{2\pi} \int \mathcal{B}(\mathbf{k}) dS_{\mathbf{k}}$ of the field $\mathcal{B} = -i \nabla_{\mathbf{k}} \times \langle \psi_+(\mathbf{k}) | \nabla_{\mathbf{k}} | \psi_+(\mathbf{k}) \rangle$ (measured in units of 2π) through a surface in momentum space surrounding the node, where $|\psi_+(\mathbf{k})\rangle$ is the state of a quasiparticle with momentum \mathbf{k} in the conduction band of a disorder-free semimetal in zero magnetic field.
- ⁴⁶ Ya. I. Rodionov and S. V. Syzranov, “Conductivity of a Weyl semimetal with donor and acceptor impurities,” *Phys. Rev. B* **91**, 195107 (2015).
- ⁴⁷ Hereinafter, the potentials $U(\mathbf{r})$ and $u(\mathbf{r})$ are the potential energies of the quasiparticles and not electrostatic potentials.
- ⁴⁸ A. A. Abrikosov, *Fundamentals of the Theory of Metals* (Elsevier, Oxford, 1988).
- ⁴⁹ V. F. Gantmakher, *Electrons and Disorder in Solids* (Oxford University Press, 2005).
- ⁵⁰ Jan Behrends and Jens H. Bardarson, “Strongly angle-dependent magnetoresistance in weyl semimetals with long-range disorder,” *Phys. Rev. B* **96**, 060201 (2017).
- ⁵¹ Sangjun Jeon, Brian B. Zhou, Andras Gyenis, Benjamin E. Feldman, Itamar Kimchi, Andrew C. Potter, Quinn D. Gibson, Robert J. Cava, Ashvin Vishwanath, and Ali Yazdani, “Landau quantization and quasiparticle interference in the three-dimensional Dirac semimetal Cd_3As_2 ,” *Nature Materials* **13**, 851 (2014).
- ⁵² Brian Skinner, “Coulomb disorder in three-dimensional Dirac systems,” *Phys. Rev. B* **90**, 060202 (2014).
- ⁵³ Wujun Shi, Benjamin J. Wieder, H. L. Meyerheim, Yan Sun, Yang Zhang, Yiwei Li, Lei Shen, Yanpeng Qi, Lexian Yang, Jagannath Jena, Peter Werner, Klaus Koepnik, Stuart Parkin, Yulin Chen, Claudia Felser, B. Andrei Bernevig, and Zhijun Wang, “A Charge-Density-Wave Weyl Semimetal,” arXiv e-prints, arXiv:1909.04037 (2019), arXiv:1909.04037 [cond-mat.mtrl-sci].
- ⁵⁴ L.D. Landau and E.M. Lifshitz, *Quantum Mechanics: Non-Relativistic Theory*, Course of Theoretical Physics (Elsevier Science, 1981).